A Deep Learning Approach to the Forward Prediction and Inverse Design of Plasmonic Metasurface Structural Color

Nathan Bryn Roberts[1] and Mehdi Keshavarz Hedayati[1, a)]
Department of Engineering, Durham University, Durham DH1 3LE, United Kingdom

(Dated: 27 July 2021)

I. ABSTRACT

This report details a deep learning approach to the forward and inverse design of plasmonic metasurface structural color. Here, optimized Deep Neural Network models are presented to enable the forward and inverse mapping between metamaterial structure and corresponding color. The forward model is capable of predicting color with >96% accuracy, with a 10^5 order of magnitude decrease in computational time when compared to finite-difference time-domain simulations used in conventional design workflows. An inverse model is trained using a tandem autoencoder, employing the pre-trained forward model. Here, the use of synthetic training data for self-learning is reported which results in $\approx 15\%$ improvement in training accuracy. The tightly constrained inverse model allows for the instantaneous design of metasurfaces, given a desired color, with an accuracy of >86%, making it suitable for commercial use as well as the acceleration of photonics research.

PACS numbers: 78.67.Pt

Metamaterials have gained significant attention in recent years for their unique ability to manipulate light in the visible spectrum. Metamaterials can be defined as artificial materials, for which their electromagnetic (EM) response is dependent on periodic subwavelength structures as opposed to intrinsic material properties[1]. Notable applications of optical metamaterials include photonic waveguides, next generation displays[1], bio sensors[2], invisibility cloaking[3], anti-counterfeit[4], information storage[5] and sustainable and high-resolution printing[678].

Periodic features on the order of hundreds of nanometers modulate light in the visible spectrum due to several physical phenomena including diffraction, resonant absorption and localized surface plasmon resonances[910]. Tuning of these features allows for frequency selec- tive absorption and scattering and hence, selective coloration. Such plasmonic metamaterials are said to exhibit structural color (SC) and have gained significant attention in recent years due to the their increasing commercial potential with ever-advancing nano-fabrication techniques[118]. The stability and recyclability of SC makes them a desirable candidate to replace current pigmentation-based printing technologies[9].

The inverse design of nanophotonic structures, meaning the design of an optimal metamaterial given a desired spectral response, would be of great commercial value, accelerating material development and the discovery of new structures. Due to the high dimensionality of the phenomena responsible for structural color, inverse design remains a challenge[12].

Conventional design workflows employ numerical simulations based on Maxwell's equations to accurately solve the EM response, given a metamaterial structure (forward mapping)[13]. Inverse design (reverse mapping) requires numerous iterations of these computationally expensive simulations in conjunction with an optimization algorithm. A review by Campbell *et al.* details numerical optimization techniques emphasising the limitations of traditional methods including the widely employed genetic algorithm (GA)[13]. Traditional methods are limited by the initial 'human guess', which drastically limits the design space and is prone to converging on local optima[13].

Deep learning (DL) is a sub-category of machine learning (ML) where multi-layer neural networks (NNs) are used for feature extraction and learning of large quantities of data, with multiple layers of abstraction[12]. Deep neural networks (DNNs) are capable of learning highly complex, non-linear relationships and have been used extensively for speech recognition, computer vision and drug discovery to name a few examples[14]. The motivation for leveraging DL is the need for a new work flow in metamaterial design, evaluating a larger parameter space and accelerating the design process.

DNN models have been reported for the forward mapping relationship between metamaterial structure and EM response, showing varying degrees of accuracy when trained on large quantities of data[1516]. The modelscan replace numerical simulations for tightly restrained structures, significantly reducing the computational burden. However, use of an optimization algorithm is needed to achieve inverse design, leading to sub-optimal convergence[13].

The inverse mapping between EM response and structure is a one-to-many relationship, meaning that multiple metamaterial configurations exhibit identical SC[17]. DNNs are one-to-one nonlinear models, hence unlike the forward relationship, DNNs cannot learn the inverse relationship directly[17]. To overcome this, sev- eral hybrid architectures have been proposed in liter-

a)mehdi.keshavarz-hedayati@durham.ac.uk

ature. Notably, a study by Liu *et al.* report the use of a tandem architecture, which allows for effective training of inverse DNNs, overcoming the fundamental issue of non-uniqueness for multi-layer thin film metamaterials[18]. Similar architectures have been reported on a limited range of metamaterials including dielectric nanorods[1920], photonic crystals[21] and other nonlinear optical applications[22]. Here, an optimised tandem architecture is presented for the inverse design of a metasurface for SC. A DL approach enables the inverse design of tightly constrained metamaterials with high accuracy.

In this work polydimethylsiloxane (PDMS) nanorod metasurfaces with aluminium (Al) coatings are used as a proof of concept for the development of DL models. Variations on this plasmonic structure have been hailed by other research groups showing desirable and robust optical properties[926]. Specifically, the use of PDMS makes these metasurfaces flexible and can allow for real-time color tuning, a promising avenue for next generation active photonic devices[1023]. In addition to the development of a practical tool for the forward and inverse design of the aforementioned structure, the methods presented here provide a generalised approach to the development of DL models for structural color.

Recent works report similar metal-dielectric nanorod materials, which are tunable across the visible spectrum and show polarization independence[26924]. As seen in figure 1(a), the structure topology consists of metal disk arrays, suspended by dielectric pillars with a metal back reflector. Structural color is observed due to selective resonant absorption by the metal structures and strong coupling between the disk and hole arrays forming hybridized reflectance modes[9]. The parameter design space includes materials, metal thickness, t, pillar diameter, d, pillar height, h, and pillar pitch, P.

Pillar pitch is fixed at 200nm to achieve angle independent viewing and a homogeneous square lattice arrangement makes the metasurface polarization independent[7924]. Table I shows the range of variables tested in this work. A total of 4620 metamaterials were simulated using a FDTD method generating a wide range of colors(*cf.* Figure 1(c)).

Feature	Range (nm)	Step (nm)	No. Simulations
Al thickness (t)	10-30	2	11
Pillar diameter (d)	38-200	6	28
Pillar height (h)	30-100	5	15
			Total: 4620

TABLE I. Range of simulated metamaterial parameters

DNNs are used for regression type problems, where both color and feature geometries take continuous values. Figure 1(b) depicts a fully connected DNN where the direction of the forward DNN (FDNN) and inverse DNN (IDNN) are indicated.

Supervised learning (SL) is the process of iteratively teaching models with labeled training data. Weights and biases are updated with each training epoch to minimize loss through methods of back propagation and gradient descent[12], where loss (cost) is defined as the Mean Squared Error (MSE) between model predictions and ground truths from labeled data.

The number of hidden layers, l and neurons in each hidden layer, n define the network architecture. In addition to architectural parameters, the choice of loss function, activation function and optimiser are all hyperparameters, which can be tuned to optimise a model for a given dataset and application.

Training data consists of tensors encoding the metamaterial structure and color, where color is calculated from reflectance spanning the visible EM spectrum. Data collection methods in previous works can be categorized by either physical experimentation or numerical simulations and are reported to be in good agreement[925]. SL of DNNs requires large data sets, making numerical simulations the favourable approach[17].

Numerical simulations were solved in the time domain using a finite-difference time-domain (FDTD) technique, based on Maxwell's equations[2627]. Here, LUMERICAL FDTD solver was used to simulate the reflectance spectra of 4620 metamaterial configurations. Table I displays the range of geometry parameters, varied within nested simulation sweeps. To maintain viewing angle independence and reduce dimensionality, a unit cell periodicity of 200nm was fixed for all materials. This allowed for use of the unit cell approximation, simulating 1/4 ofone nanorod with symmetrical boundaries. 50-point discretized reflectance spectra were collected for each material between 400 and 750nm. PDMS was defined using a refractive index value of 1.41 (assumed to be constant across the visible spectrum)[28]. Al properties were defined using frequency dependent permittivity from the handbook of Palik[29].

A method of parameter vectorisation was used to encode the metamaterial structures, where pillar diameter, height and Al thickness take numerical values ranging between 5 and 200nm. To enable effective learning with gradient decent algorithms, features were individually normalised (*c.f* SI).

Direct interpretation of the metamaterial reflectance spectra cannot provide an intuitive indication of perceived color. For use as a practical design tool, dimensionallity reduction to the CIE 1931 chromaticity gamut was used to encode SC chromaticity[24430] (*c.f* SI).

The resultant colors from all simulated metamaterials are seen in Figure 1(c). The metamaterials display a broad gamut of colors spanning far from the achromaitic point, showing highly saturated examples of blue, purple, pink, orange and yellow. This material topology struggles to produce highly saturated green and red colors originating from spectral dips due to resonant absorption[9].

Encoded simulation data were shuffled and randomly split into training and test sets with a ratio of 80:20, where 20% of the training set was used for validation during learning. A pseudorandom seed was used to provide repeatable pseudorandom test sets for the development of models and meaningful comparison of performance metrics.

Here, an optimised FDNN model is presented, which

FIG. 1. (a) Metasurface composed of polymeric pillar (PDMS) with metal coating (Al). Pitch, metal thickness, height and pillar diameter are *P, t, h* and *d*, respectively. (b) Fully connected DNN, where *l* and *n* are the number of hidden layers and neurons in each hidden layer, respectively. (c) Range SCs from simulated metamaterials plotted on CIE 1931 gamut.

FIG. 2. (a) Learning curve of FDNN model showing validation and training cost as a function of epochs, where cost is defined as the MSE between model predictions and ground truths. (b) CIE 1931 scatter plot showing FDNN model predictions on the test set, where blue and red dots indicate the model predictions and ground truths, respectively.

FIG. 3. Autoencoder architecture used for IDNN training, where CIE input and output tensors encode desired and predicted color respectively.

allows for the prediction of color given a metamaterial structure. The following sections provide details of the model optimisation and development.

As observed in Figure 1(c), a large quantity of the simulated metamaterials are clustered around the achromatic CIE point, where low color saturation and broadband reflectance is observed. Early models showed ability to predict colors around this cluster with high accuracy, however failed to predict highly saturated colors at the extremities (with fewer training samples). This is because trainable parameters are skewed toward data clusters when using an averaged loss metric. To overcome this, data centered around the achromatic point were removed using a square mask. The data set was reduced from 4620 to 2394 samples and used for all subsequent model development (*c.f* SI).

An experiment was undertaken in which 160 different model architecture permutations were trained, each for three independent trials (*c.f* SI). The optimum network architecture was found to be 7 hidden layers, each with 950 neurons employing ReLU activation functions. Furthermore, MSE loss function and Keras's Adam optimiser were used.

The FDNN model was trained for a total of 4795 epochs. Figure 2(a) shows the learning curve, where training accuracy converges to 98.57%. Validation losses are in good agreement, indicating a well-fit model. When evaluated on the test set, color predictions were 96.03% accurate, where accuracy is defined as the MSE between model predictions and ground truths. Figure 2(b) displays a qualitative representation of test accuracy, showing the model's ability to predict colors across the gamut.

The FDNN model can be used to replace numerical simulations in the forward design process and critically provides a 10^5 order of magnitude decrease in computational time when compared to FDTD simulations. In addition, the FDNN model may be used as a sub-optimal inverse design tool when an external optimisation method such as GA is used[13].

To overcome the issue of non-uniqueness for the inverse design problem, a tandem autoencoder architecture is employed[18,21,22]. Figure 3 shows a diagram of the learning architecture, where the pretrained forward model is used to train an inverse DNN. The loss is defined as the MSE between the desired color (input vector) and predicted color (output vector). The hidden layer joining the two networks is three neurons deep, representing the latent encoding of geometry parameters *d, h,* and *t*. The weights of the FDNN are frozen and is used to predict color from the geometry vector output of the IDNN. The tandem model is trained using back propagation and gradient decent (Keras Adam optimiser) to minimize the loss between the desired color and the model prediction. Since the input to the FDNN is a vector of geometries, the inverse network learns to design metamaterial parameters *d, h, t* for target colors. This training method overcomes the fundamental issue of non uniqueness because the metamaterial structures are not limited to those in a finite labeled training set[18]. Once trained, the IDNN is separated from the tandem structure and used as a stand-alone model.

The optimum IDNN architecture was found to be 4 hidden layers, each with 950 neurons employing ReLU activation functions. Use of sigmoid activation functions (equation 1) in the final IDNN layer of 3 neurons, bounds the output between 0 and 1. This restricts the predicted geometries within the range of simulated features in the training set due to feature normalisation (*c.f* Table I). This is a necessary optimization, as unconstrained IDNN models predicted nonphysical metamaterials including negative dimensions and pillar diameters exceeding the unit cell.

$$\sigma(a) = \frac{1}{1 + e^{-a}} \tag{1}$$

Autoencoder architectures enable unsupervised self-learning. Here, the first reported use of unlabeled, synthetic training data leads to an approximate 15% increase in training accuracy. Previous works[18,19,20] report the training of similar architectures using labeled simulation data. Due to the dimensionality reduction of color to the 2D CIE domain, here, arbitrarily large sets of random colors without corresponding structures can be used in training. The unlabeled training set consisted of 20,000 random colors, generated to be within ± 0.01 of colors corresponding to the simulated metamaterials, in both CIE x and y directions (*c.f* SI). This leads to improved learning and enables the IDNN model to design metasurfaces with a larger range of SCs (*c.f* SI). Figure 4(a) displays the learning curves of the IDNN where a training

accuracy of 87.55% is achieved.

FIG. 4. (a) Learning curve of IDNN model showing valida- tion and training cost as a function of epochs, where cost is defined as the MSE between model prediction and desired color. (b) Evaluation of the IDNN tandem model using 5000 random colors. For visual aid, 500 model predictions are plot-ted on the CIE 1931 gamut, where target colors and model predictions are seen in red and blue, respectively.

Evaluation of the inverse model is challenging due to the many-to-one relationship. The inverse model may accurately predict a metamaterial structure for a given color, which is different to the structure in the test set. This is the same reason why direct training of IDNNs is not possible. Hence, comparing the IDNN-designed metamaterial parameters; *d, h, t,* with the simulated test set does not provide a suitable method of evaluation.

Instead, 5000 randomly sampled 'unseen' colors were used as a test set. The corresponding IDNN-designed metamaterials were validated using the FDNN model in the tandem architecture depicted in Figure 3. The test accuracy was then calculated as the MSE between target colors and those predicted by the FDNN. Figure 4(b) is a visual representation of this evaluation metric, where the IDNN model designed metamaterials with an accuracy of 89.80%.

This approach provides a rapid and repeatable method for the evaluation of IDNNs, however, use of the imperfect FDNN leads to compounding uncertainties. The FDNN has a test accuracy of 96.03% and thus a more realistic estimate of the IDNN model's accuracy is 86.21%.

To provide additional confidence in the IDNN model, an absolute accuracy metric was obtained by individually verifying the colors of inversely designed metamaterials. As seen in Figure 5, 10 metamaterials were designed using the IDNN, given random target colors. The metamaterials were subsequently verified using FDTD methods and the corresponding 'true' color of each metamaterial is compared to the target color.

It is apparent from the small test set, that the IDNN model is able to design metamaterials with high precision, spanning blue, purple and pink colors. However, trials 1, 6-7 indicate a systematic error in the design of orange-hued metasurfaces. This implies that the quoted error of 86.21% is not randomly distributed across the color gamut. This systematic error is due to the compounding uncertainty introduced by the imperfect FDNN during training. Figure 4(b), provides a qualitative insight to this systematic error where a predictive dead-zone is observed between $0.35 - 0.425$ and $0.35 - 0.45$ in CIE x and y directions, respectively. This was observed in all IDNN models trained with the same FDNN.

FIG. 5. Evaluation of 10 IDNN-designed metamaterials where random target SCs are compared to the true SC. CIE 1931 x,y coordinates of both target colors and designed colors are displayed.

These results provide confidence in the presented DL method as a practical tool for the instantaneous design of metamaterials. The model is able to accurately design SCs different to those in the original training data and thus interpolating the complex relationship between color and structure. Caution however, should be taken when using the inverse model and the proposed evaluation metrics presented in Figures 4(b) and 5 provide valuable insight to the limitations of the statistical model. Full-wave simulations should be used to verify the inverse model's designs before they are taken to be true.

A trend in recent works, has been the anecdotal validation of inverse model performance using few selected examples[18,19,20]. Although this provides excitement within the community, it serves little in the way of providing confidence in DL methodologies and cannot be used to justify one inverse architecture over another. Here, an additional accuracy metric based on the autoencoder model was proposed (*c.f* Figure 4(b)), which provides a rapid performance metric to aid model development and hyperparameter tuning and provides additional insight to the IDNN performance.

A DL approach to the forward and inverse design of photonic metamaterials was reported. Here, metal-dielectric nanorod metasurfaces composed of Al and PDMS were simulated using a FDTD method, displaying a wide range structural colors. Due to the flexibility of PDMS, these metamaterials have applications in real-time tunable color and are hailed as promising candidates for next generation screen technologies. In addition, the use of Al makes the metamaterial a sustainable and low cost alternative to metamaterials commonly employing Ag and Au.

A DL model was developed for the forward map-ping between structure and color and can replace full- wave EM simulations with a 10^5 order of magnitude de-crease in computational burden and a predictive accu- racy of >96%. Moreover, the fundamental issue of non-uniqueness for the training of inverse models was overcome through the use of an autoencoder architecture with a pre-trained forward model. The tightly restrained inverse model can be used to design metamaterials, given desired colors with an accuracy of approximately 86%. The first reported use of un-labeled self learning with synthetic data allowed the autoencoder model to make use of large training data and improved the training accuracy by approximately 15%. In addition to the development of metamaterial-specific models, the methods presented here provide a generalised approach to the design of complex metamaterials using deep learning.

SUPPLEMENTARY INFORMATION

See Supplementary Information (SI) for details of data acquisition, data encoding methods and supporting ma-

terial on the development and evaluation of DL models.

ACKNOWLEDGMENTS

The authors would like to acknowledge the financial support from the Department of Engineering, Durham University.

DATA AVAILABILITY STATEMENT

The data that support the findings of this study are openly available in Zenodo, reference number 10.5281/zenodo.5102770.

II. REFERENCES

[1]S. D. Rezaei, Z. Dong, J. Y. E. Chan, J. Trisno, R. J. H. Ng, Q. Ruan, C.-W. Qiu, N. A. Mortensen, and J. K. Yang, " Nanophotonic structural colors," ACS Photonics **8**, 18–33 (2021).

[2]K. Raman, T. S. Murthy, and G. Hegde, " Fabrication of re- fractive index tunable polydimethylsiloxane photonic crystal for biosensor application," Physics Procedia **19**, 146–151 (2011).

[3]W. Cai, U. K. Chettiar, A. V. Kildishev, and V. M. Shalaev, " Optical cloaking with metamaterials," Nature photonics **1**, 224–227 (2007).

[4]A. Ruiz-Clavijo, Y. Tsurimaki, O. Caballero-Calero, G. Ni, G. Chen, S. V. Boriskina, and M. Martín-González, " Engineering a full gamut of structural colors in all-dielectric mesoporous network metamaterials," ACS Photonics **5**, 2120–2128 (2018).

[5]F. Cheng, J. Gao, L. Stan, D. Rosenmann, D. Czaplewski, and X. Yang, "Aluminum plasmonic metamaterials for structural color printing," Optics express **23**, 14552–14560 (2015).

[6]R. J. H. Ng, S. J. Tan, X. M. Goh, and J. K. W. Yang, "Plasmonic color printing," in *2015 9th International Congress on Advanced Electromagnetic Materials in Microwaves and Optics (METAMATERIALS)* (2015) pp. 328–330.

[7]F. Cheng, J. Gao, L. Stan, D. Rosenmann, D. Czaplewski, and X. Yang, " Aluminum plasmonic metamaterials for structural color printing," Optics Express **23**, 14552 (2015).

[8]X. Zhu, M. K. Hedayati, S. Raza, U. Levy, N. A. Mortensen, and A. Kristensen, " Digital resonant laser printing: Bridging nanophotonic science and consumer products," Nano Today **19**, 7–10 (2018).

[9]J. S. Clausen, E. Højlund-Nielsen, A. B. Christiansen, S. Yazdi, M. Grajower, H. Taha, U. Levy, A. Kristensen, and N. A. Mortensen, " Plasmonic metasurfaces for coloration of plastic con- sumer products," Nano letters **14**, 4499–4504 (2014).

[10]M. K. Hedayati and M. Elbahri, "Review of metasurface plasmonic structural color," Plasmonics **12**, 1463–1479 (2016).

[11]E. Højlund-Nielsen, J. Clausen, T. Mäkela, L. H. Thamdrup, M. Zalkovskij, T. Nielsen, N. Li Pira, J. Ahopelto, N. A. Mortensen, and A. Kristensen, " Plasmonic colors: toward mass production of metasurfaces," Advanced Materials Technologies **1**, 1600054 (2016).

[12]J. Jiang, M. Chen, and J. A. Fan, " Deep neural networks for the evaluation and design of photonic devices," Nature Reviews Materials (2020), 10.1038/s41578-020-00260-1.

[13]S. D. Campbell, D. Sell, R. P. Jenkins, E. B. Whiting, J. A. Fan, and D. H. Werner, " Review of numerical optimization techniques for meta-device design," Opt. Mater. Express **9**, 1842–1863 (2019).

[14]Y. Lecun, Y. Bengio, and G. Hinton, "Deep learning," Nature **521**, 436–444 (2015).

[15]W. Ma, Z. Liu, Z. A. Kudyshev, A. Boltasseva, W. Cai, and Y. Liu, " Deep learning for the design of photonic structures," Nature Photonics , 1–14 (2020).

[16]Y. Xu, X. Zhang, Y. Fu, and Y. Liu, "Interfacing photonics with artificial intelligence: an innovative design strategy for photonic structures and devices based on artificial neural networks," Photonics Research **9**, B135–B152 (2021).

[17]R. S. Hegde, "Deep learning: a new tool for photonic nanostructure design," Nanoscale Advances **2**, 1007–1023 (2020).

[18]D. Liu, Y. Tan, E. Khoram, and Z. Yu, " Training deep neural networks for the inverse design of nanophotonic structures," ACS Photonics **5**, 1365–1369 (2018).

[19]L. Gao, X. Li, D. Liu, L. Wang, and Z. Yu, "A bidirectional deep neural network for accurate silicon color design," Advanced Materials **31**, 1905467 (2019).

[20]I. Tanriover, W. Hadibrata, and K. Aydin, "Physics-based approach for a neural networks enabled design of all-dielectric metasurfaces," ACS Photonics **7**, 1957–1964 (2020).

[21]C.-X. Liu, G.-L. Yu, and G.-Y. Zhao, "Neural networks for inverse design of phononic crystals," AIP Advances **9**, 085223 (2019), https://doi.org/10.1063/1.5114643.

[22]B. Rahmani, D. Loterie, E. Kakkava, N. Borhani, U. Teğin, D. Psaltis, and C. Moser, " Actor neural networks for the ro- bust control of partially measured nonlinear systems showcasedfor image propagation through diffuse media," Nature Machine Intelligence **2**, 403–410 (2020).

[23]Z. Xu, "A stretchable terahertz parabolic-shaped metamaterial," Advanced Optical Materials **7**, 1900379 (2019).

[24]E. Højlund-Nielsen, J. Weirich, J. Nørregaard, J. Garnaes, N. A. Mortensen, and A. Kristensen, " Angle-independent structural colors of silicon," Journal of Nanophotonics **8**, 083988 (2014).

[25]J. Baxter, A. C. Lesina, J.-M. Guay, A. Weck, P. Berini, and L. Ramunno, " Plasmonic colours predicted by deep learning," Scientific Reports **9** (2019), 10.1038/s41598-019-44522-7.

[26]V. Caligiuri, G. Tedeschi, M. Palei, M. Miscuglio, B. Martin-Garcia, S. Guzman-Puyol, M. K. Hedayati, A. Kristensen, A. Athanassiou, R. Cingolani, V. J. Sorger, M. Salerno, F. Bonaccorso, R. Krahne, and J. A. Heredia-Guerrero, " Biodegradableand insoluble cellulose photonic crystals and metasurfaces," ACS Nano **14**, 9502–9511 (2020).

[27]W. Ma, F. Cheng, Y. Xu, Q. Wen, and Y. Liu, "Probabilistic representation and inverse design of metamaterials based on adeep generative model with semi-supervised learning strategy," Advanced Materials **31**, 1901111 (2019).

[28]Z. Cai, W. Qiu, G. Shao, and W. Wang, "A new fabrication method for all-pdms waveguides," Sensors and Actuators A: Physical **204**, 44–47 (2013).

[29]E. D. Palik, *Handbook of optical constants of solids*, Vol. 3 (Academic press, 1998).

[30]Z. Huang, X. Liu, and J. Zang, " The inverse design of struc- tural color using machine learning," Nanoscale **11**, 21748–21758 (2019).

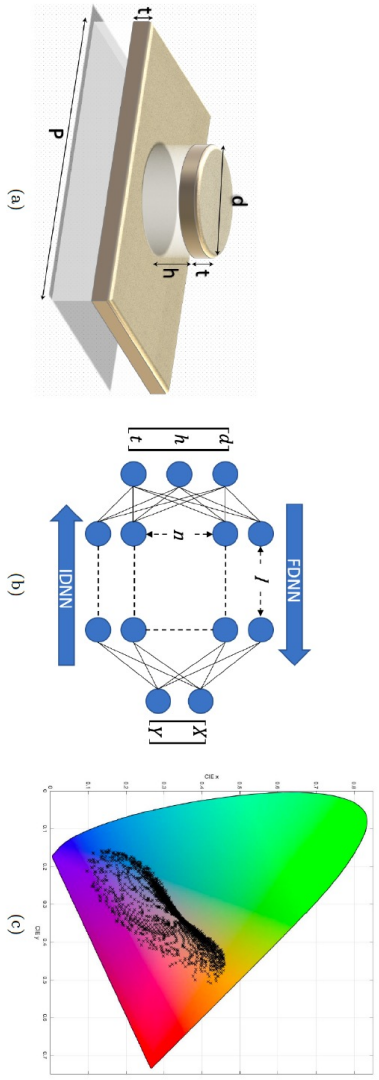

PLEASE CITE THIS ARTICLE AS DOI: 10.1063/5.0055733

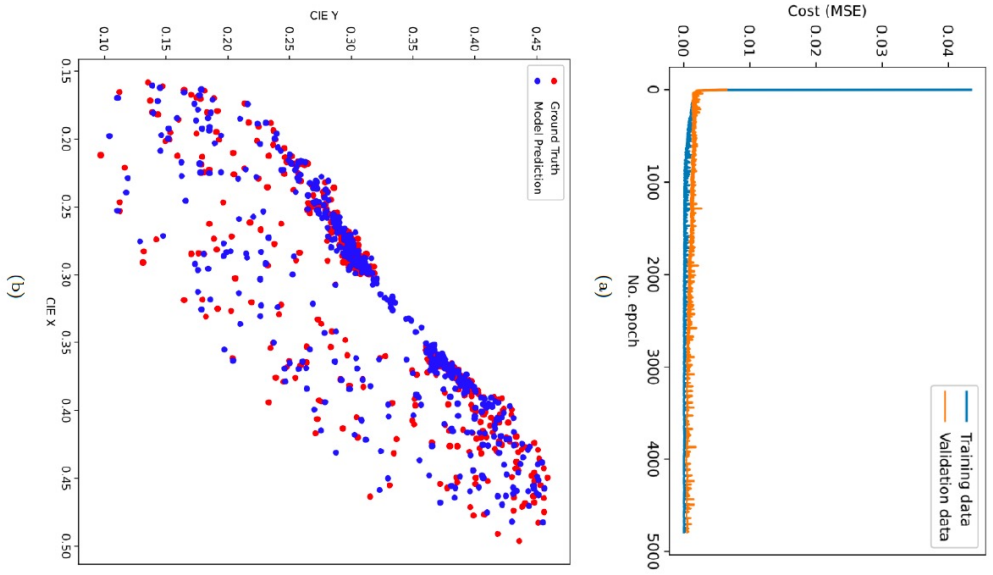

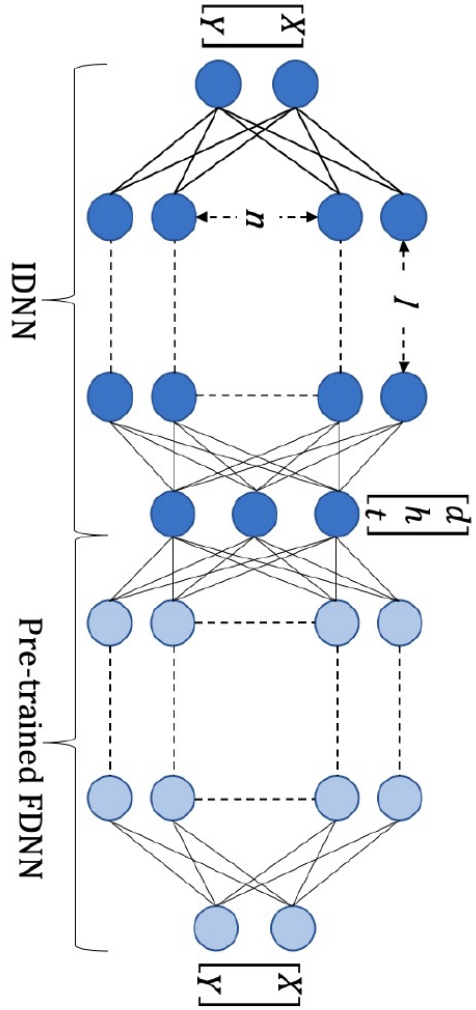

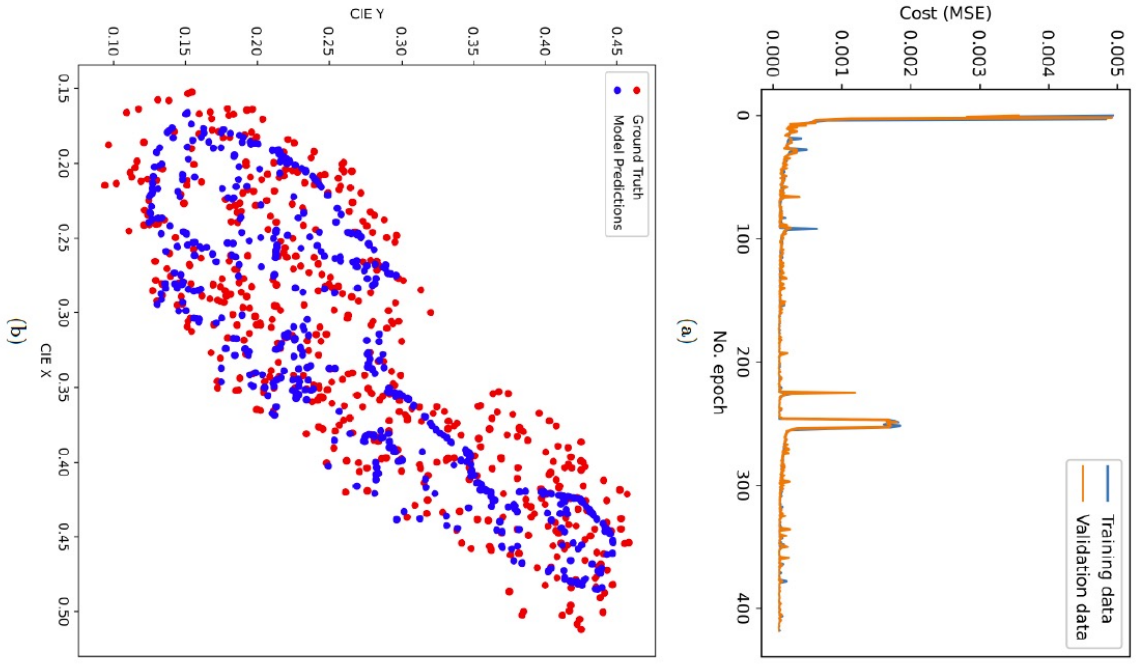

	Target color	Designed color	Error (1931 CIE)	
			Δ CIE x	Δ CIE y
1	0.4823, 0.3953	0.3593, 0.2101	0.1230	0.1852
2	0.1633, 0.1560	0.1662, 0.1309	0.0029	0.0251
3	0.3468, 0.2115	0.3562, 0.1934	0.0094	0.0181
4	0.3945, 0.2688	0.4088, 0.2665	0.0144	0.0023
5	0.4242, 0.3152	0.4159, 0.2821	0.0083	0.0331
6	0.5032, 0.4392	0.3446, 0.2020	0.1586	0.2372
7	0.4861, 0.4115	0.3566, 0.2106	0.1295	0.2009
8	0.2631, 0.1997	0.2496, 0.1070	0.0135	0.0927
9	0.2611, 0.1676	0.2933, 0.1318	0.0322	0.0358
10	0.4539, 0.3183	0.4410, 0.3484	0.0130	0.0301